



Structural insights into Ras regulation by SIN1

Yuyuan Zheng^{a,b,c,1}, Lei Ding^{a,b,1}, Xianhui Meng^c, Meg Potter^d, Alison L. Kearney^d, Jie Zhang^{a,b}, Jie Sun^c, David E. James^{d,e}, Guang Yang^{d,2,3}, and Chun Zhou^{a,b,3}

Edited by Dafna Bar-Sagi, New York University Langone Health, New York, NY; received November 2, 2021; accepted April 5, 2022

Over the years it has been established that SIN1, a key component of mTORC2, could interact with Ras family small GTPases through its Ras-binding domain (RBD). The physical association of Ras and SIN1/mTORC2 could potentially affect both mTORC2 and Ras-ERK pathways. To decipher the precise molecular mechanism of this interaction, we determined the high-resolution structures of HRas/KRas-SIN1 RBD complexes, showing the detailed interaction interface. Mutation of critical interface residues abolished Ras-SIN1 interaction and in SIN1 knockout cells we demonstrated that Ras-SIN1 association promotes SGK1 activity but inhibits insulin-induced ERK activation. With structural comparison and competition fluorescence resonance energy transfer (FRET) assays we showed that HRas-SIN1 RBD association is much weaker than HRas-Raf1 RBD but is slightly stronger than HRas-PI3K RBD interaction, providing a possible explanation for the different outcome of insulin or EGF stimulation. We also found that SIN1 isoform lacking the PH domain binds stronger to Ras than other longer isoforms and the PH domain appears to have an inhibitory effect on Ras-SIN1 binding. In addition, we uncovered a Ras dimerization interface that could be critical for Ras oligomerization. Our results advance our understanding of Ras-SIN1 association and crosstalk between growth factor-stimulated pathways.

Ras | SIN1 | PI3K | insulin | mTORC2

The mechanistic target of rapamycin (mTOR) is a master protein kinase that forms two distinct protein complexes: mTORC1 (mTOR, Raptor, mLST8, and PRAS40) and mTORC2 (mTOR, Rictor, mLST8, SIN1, and Protor1/2) (1–3). mTORC1 integrates signals such as amino acids, growth factors, stress, and energy status to regulate major cellular processes including growth, proliferation, and survival while mTORC2 transduces signals from growth factors to pathways involved in proliferation, cytoskeletal organization, and anabolic output. Disturbance of mTOR signaling pathways results in many human diseases including cancer (2, 4, 5).

It has long been established that various small GTPases like Rheb or Rag directly or indirectly regulate mTORC1 activity (6–10). Early studies in *Saccharomyces cerevisiae* and *Dictyostelium* clearly revealed the association of Ras orthologous with SIN1, an essential component of TORC2 (11, 12). Later it was shown that human SIN1 contains a Ras-binding domain and colocalizes with HRas and KRas (13). Recently it has been reported that Ras family small GTPases could directly bind to mTORC2 through SIN1 and disruption of the mTORC2 association with mutant NRas, HRas, or KRas impairs Ras-driven tumorigenesis (14). SIN1 is specific to mTORC2 and helps to regulate mTORC2 kinase specificity toward AGC family kinases (15–19). It has an N-terminal domain involved in Rictor binding, followed by the CRIM, Ras-binding (RBD), and pleckstrin homology-like (PH) domains. The latter three domains are flexibly tethered to the N-terminal domain and not observed in the cryo-electron microscopy structure of the mTORC2 complex (20). To better understand the molecular mechanism and functional outcome of SIN1-Ras association, we carried out a series of biochemical and structural studies of SIN1 and Ras complex.

Results

In vitro isothermal titration calorimetry (ITC) binding assays demonstrated that SIN1 RBD preferentially binds Ras G domains rather than other small GTPases, such as RhoA or Rac1 (Fig. 1 *A* and *B* and *SI Appendix*, Figs. *S1* and *S2*). GST pull-down experiments further validated that SIN1 RBD could interact with HRas, KRas, and NRas G domains (*SI Appendix*, Fig. *S3*). We next determined crystal structures of GMPPNP-bound HRas wild-type (WT) G domain in complex with SIN1 RBD at 1.6 Å resolution (Fig. 1 *C* and *D* and *SI Appendix*, Fig. *S4A* and Table *S1*). SIN1 RBD is composed of two α -helices and four β -strands and adopts a ubiquitin-like fold, similar to other RBDs (Fig. 1 *C* and *SI Appendix*, Fig. *S2*). β -strands 1, 2 from

Significance

Both the mTORC2 and Ras-ERK pathways respond to growth factor stimulation and play critical roles in cell growth and proliferation, disarray of these pathways leads to many diseases, especially cancer. These two signaling pathways crosstalk at many levels; recently it's become clear that the SIN1 component of mTORC2 could interact with Ras family small GTPases, but how these two proteins interact at the molecular level and the functional outcomes of this interaction remain to be addressed. In this work we determined the high-resolution structure of Ras-SIN1 complexes and revealed the detailed interaction mechanism. We also showed that Ras-SIN1 association inhibits insulin-induced ERK activation. Insights from this work could improve our understanding of the disease-causing mechanism of errant mTORC2 or Ras proteins.

Author contributions: J.S., D.E.J., G.Y., and C.Z. designed research; Y.Z., L.D., X.M., M.P., A.L.K., J.Z., G.Y., and C.Z. performed research; J.S., D.E.J., G.Y., and C.Z. analyzed data; and Y.Z., G.Y., and C.Z. wrote the paper.

The authors declare no competing interest.

This article is a PNAS Direct Submission.

Copyright © 2022 the Author(s). Published by PNAS. This article is distributed under [Creative Commons Attribution-NonCommercial-NoDerivatives License 4.0 \(CC BY-NC-ND\)](https://creativecommons.org/licenses/by-nc-nd/4.0/).

¹Y.Z. and L.D. contributed equally to this work.

²Present address: School of Biotechnology and Biomolecular Sciences, The University of New South Wales, Sydney, NSW 2052, Australia.

³To whom correspondence may be addressed. Email: chunzhou@zju.edu.cn or guang.yang7@unsw.edu.au.

This article contains supporting information online at <http://www.pnas.org/lookup/suppl/doi:10.1073/pnas.2119990119/-DCSupplemental>.

Published May 6, 2022.

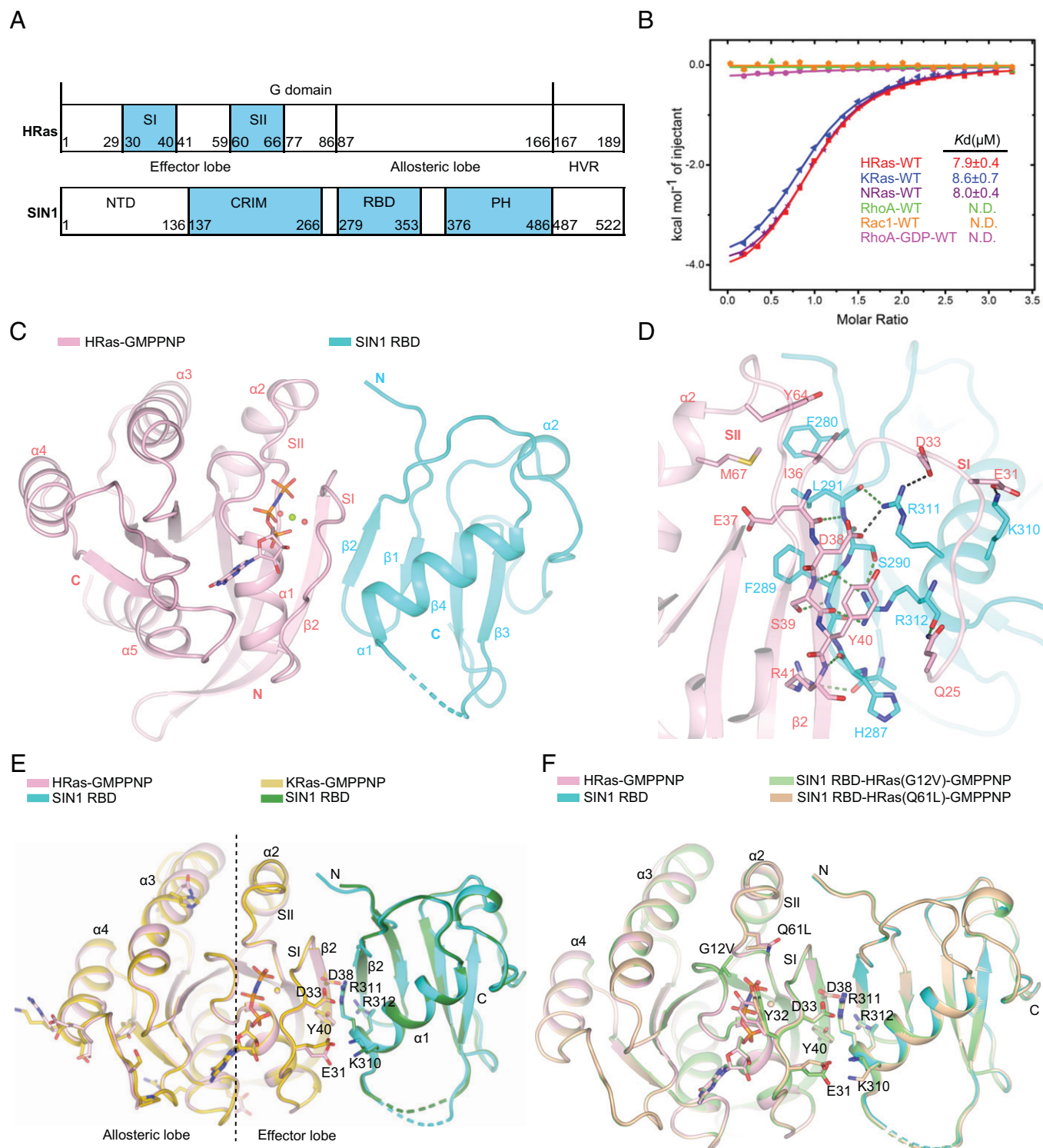


Fig. 1. Structure of Ras-SIN1 RBD complexes. (A) Linear domain diagrams of HRas and SIN1. (B) ITC titration results of SIN1 RBD with different small G proteins. (C) The 1.6-Å crystal structure of HRas-GMPPNP in complex with SIN1 RBD. Green sphere is Mg^{2+} , red spheres are water molecules, GMPPNP is shown as sticks. SI, Switch I region; SII, Switch II region. (D) Close-up view of HRas-SIN1 RBD interaction interface. Green dashed lines indicate hydrogen bonds, black dashed lines denote salt bridges. (E) Superposition of HRas-SIN1 RBD structure with KRas-SIN1 RBD structure. The residues that are different between HRas and KRas are located in the allosteric lobe and not involved in SIN1 RBD interaction. (F) Superposition of HRas-SIN1 RBD structure with HRas(G12V)-SIN1 RBD and HRas(Q61L)-SIN1 RBD structures. The three structures are nearly identical with minor differences.

SIN1 RBD form an antiparallel β -sheet with HRas β -strands 2, 3, mostly through main-chain hydrogen bonding (Fig. 1D). Above the β -sheet, a few conserved and positively charged residues from SIN1 RBD α 1 form salt bridges and hydrogen bonds with residues from the HRas Switch I region. Specifically, positively charged R311 is sandwiched between D38

and D33, while R312 forms hydrogen bonds with several main-chain carbonyl groups and stacks against Y40 through cation- π interaction (Fig. 1D). Near the Switch II region, several hydrophobic residues from SIN1 RBD (L291, F280) pack against a hydrophobic patch formed by Y64, M67, and I36 (Fig. 1D).

We also determined structures of the KRas WT, HRas G12V, or Q61L G domain in complex with SIN1 RBD (Fig. 1 *E* and *F* and *SI Appendix*, Table S1). KRas interacts with SIN1 RBD in a similar way to HRas. Alignment of KRas-SIN1 RBD structure with HRas-SIN1 RBD structure yielded an rmsd of 0.35 Å over 241 C α atoms as KRas and HRas share 95% sequence identity (Fig. 1*E* and *SI Appendix*, Fig. S1). Residues that are different between KRas and HRas are located in the allosteric lobe, which is away from the interaction interface (Fig. 1*E*). HRas G12V and Q61L structures are nearly identical to the WT structure (Fig. 1*F*). In the mutant structures, the Y32 side chain is rotated closer and forms a direct hydrogen bond with the phosphate group of GMPPNP as observed previously (21) (Fig. 1*F*). ITC titrations show that HRas G12V binds SIN1 RBD with higher affinity than WT HRas, while Q61L binding is slightly weaker than that of WT HRas (*SI Appendix*, Fig. S4*B*).

To probe the function of SIN1-Ras interaction, we generated several mutations of R311 and R312. ITC binding assays, GST pull-down, and fluorescence resonance energy transfer (FRET) experiments demonstrated that these mutations partially or near completely abolished SIN1 RBD/HRas binding in vitro (Fig. 2*A* and *SI Appendix*, Fig. S5 *A* and *B*). The pivotal role of R311 in the interaction of SIN1 RBD and Ras was further validated by Co-immunoprecipitation (Co-IP) of SIN1 and HRas in cells (Fig. 2*B*). To clarify the consequence of the SIN1-Ras association, we expressed SIN1 WT and R311 mutants in SIN1 knockout mouse embryonic fibroblasts (MEFs). While a recent study showed that Ras interaction with SIN1 is dispensable for mTORC2 activity in regard to Akt and PKC α phosphorylation (22), in SIN1 knockout MEFs, we found that reexpression of SIN1 R311K or R311A mutant led to less phosphorylation of NDRG1 (a substrate of SGK1 kinase) than reexpression of SIN1 WT despite less WT SIN1 expressed (Fig. 2 *C* and *D*), indicating Ras interaction with SIN1 could promote SGK1 activity. SIN1 protein contains a CRIM domain (Fig. 1*A*), which was demonstrated to bind Akt (23). With purified proteins, we showed that GST-tagged SIN1 CRIM domain pulled down a significant amount of SGK1 kinase domain while a poly NQ mutant in the CRIM domain nearly abolished the interaction between CRIM and SGK1 (*SI Appendix*, Fig. S6*A*). The poly NQ mutant was previously shown to disrupt interaction between CRIM and Akt (23). The presence of the RBD and the PH domain appears to have little effect on the interaction between CRIM and SGK1 (*SI Appendix*, Fig. S6*A*). To see whether Ras-RBD binding could promote CRIM-SGK1 association, we used GST-tagged WT and mutant CRIM-RBD to pull down SGK1 and HRas-GMPPNP (*SI Appendix*, Fig. S6*B*). HRas did not cause significant change to CRIM-SGK1 interaction. So the increased SGK1 activity is not likely due to synergistic binding of Ras and SGK1 to SIN1. The interpretation of the effect of Ras-SIN1 association on Akt is complicated by less WT SIN1 expression than mutants in our stably transfected MEF cells (Fig. 2 *C* and *E*).

We also found that under insulin stimulation, reexpression of WT SIN1 substantially suppressed phosphorylation of ERK, but R311-mutated SIN1 partially lost this inhibitory effect. Intriguingly, SIN1 does not suppress EGF-induced ERK phosphorylation (Fig. 2*E*). The time course experiments demonstrated that SIN1 indeed inhibits the maximum phosphorylation of ERK induced by insulin rather than delays its activation (Fig. 2 *F–J*). These data indicate that the interaction

of SIN1 and Ras inhibits MAPK signaling only in response to specific growth factors.

Raf, a well-established Ras effector, plays critical roles in growth factor-stimulated ERK phosphorylation (24). To see whether there is any competition between SIN1-HRas interaction and Raf1-HRas interaction, which would in theory inhibit ERK phosphorylation, we first compared HRas-SIN1 RBD interaction with the HRas-Raf1 RBD complex (25). In vitro, HRas interacts with the Raf1 RBD with much higher affinity ($K_d \sim 0.2$ to $0.3 \mu\text{M}$), 40 times higher, than with the SIN1 RBD (Figs. 1*B* and 3*C*). After superposition of the structures, we found that the Raf1 RBD interacts with the Switch I loop of HRas similarly to SIN1 RBD, with K84, R89 on Raf1 interacting with E31, D33, D38, and Y40 on HRas (Fig. 3*A*). However, at the rear of the β -sheet formed between the HRas-Raf1 RBD, Raf1 R67 and R59 formed strong electrostatic interactions with HRas E37. In the SIN1 RBD, R282 (R59 equivalent) is 5.4 Å away from E37, and R67 in Raf1 is replaced with F289 (Fig. 3*B*). Furthermore, the existence of a shorter valine (V69) in Raf1 instead of a longer leucine (L291 in SIN1) allowed close contact of E37 with R59 (Fig. 3*B*). Although replacing R67 with F in Raf1 RBD only slightly weakened the binding affinity for HRas, further mutation of Raf V69 to L greatly reduced HRas-Raf1 RBD affinity (15-fold reduction, Fig. 3*C*). In a FRET competition assay, an equal molar amount of WT Raf1 RBD strongly competed with SIN1 RBD and nearly abolished the FRET between SIN1 RBD-ECFP and YPet-HRas, and double-mutant Raf1 RBD could still compete with SIN1 RBD but to a lesser extent (Fig. 3*D*). So it is unlikely that SIN1 directly competes with Raf1 for Ras binding.

PI3K is another well-described Ras effector (26, 27). Analysis of the PI3K γ -HRas complex structure showed that PI3K γ mostly uses its RBD region to interact with HRas (28) and the interaction mode is analogous to that of Raf1 RBD or SIN1 RBD (Fig. 3 *E* and *F* and *SI Appendix*, Fig. S7*A*). PI3K γ RBD uses K255, K251 to coordinate HRas D33 while Q231 forms two hydrogen bonds with Y40 and D38. HRas E31 appears to be not involved in the interaction with PI3K γ RBD (Fig. 3*E*). At the rear side of the β -sheet, due to the smaller size of PI3K γ S230 side chain, PI3K γ K223 was able to form a salt bridge with HRas E37 (Fig. 3*F*). Alignment of Raf1 RBD-HRas and PI3K γ RBD-HRas structures with SIN1 RBD-HRas revealed that HRas conformation is quite similar in all three structures while different RBDs bind to HRas with slightly rotated angles (*SI Appendix*, Fig. S7*A*). In vitro, PI3K γ RBD displayed a K_d around 6.2 μM for HRas-GMPPNP, slightly stronger than SIN1 RBD (8.1 μM) (Fig. 3*G*). On the other hand, PI3K α is measured to bind HRas-GMPPNP with a K_d around 14 μM (Fig. 3*G*). In FRET competition assays we found that either SIN RBD or PI3K RBDs could compete with each other (Fig. 3 *H* and *I* and *SI Appendix*, Fig. S7 *B* and *C*). However, in all experiments, SIN1 RBD inhibits the FRET signal more than PI3K α , PI3K γ RBDs, indicating SIN1 RBD is preferred for HRas binding under similar conditions. Importantly, SIN RBD R311A mutant failed to compete with SIN RBD or PI3K RBDs (Fig. 3 *H* and *I*), in agreement with our findings in Fig. 2. An equal amount of Raf1 RBD significantly inhibited HRas binding to SIN1 RBD or PI3K RBDs due to its high affinity (Fig. 3 *D*, *H*, and *I* and *SI Appendix*, Figs. S7 *B* and *C*). These in vitro observed affinity differences might help to explain how Ras differentiates its effectors and provide important clues about the crosstalk between different pathways. A previous study showed that insulin-induced ERK1/2 phosphorylation was very sensitive to PI3K-specific inhibitors, wortmannin

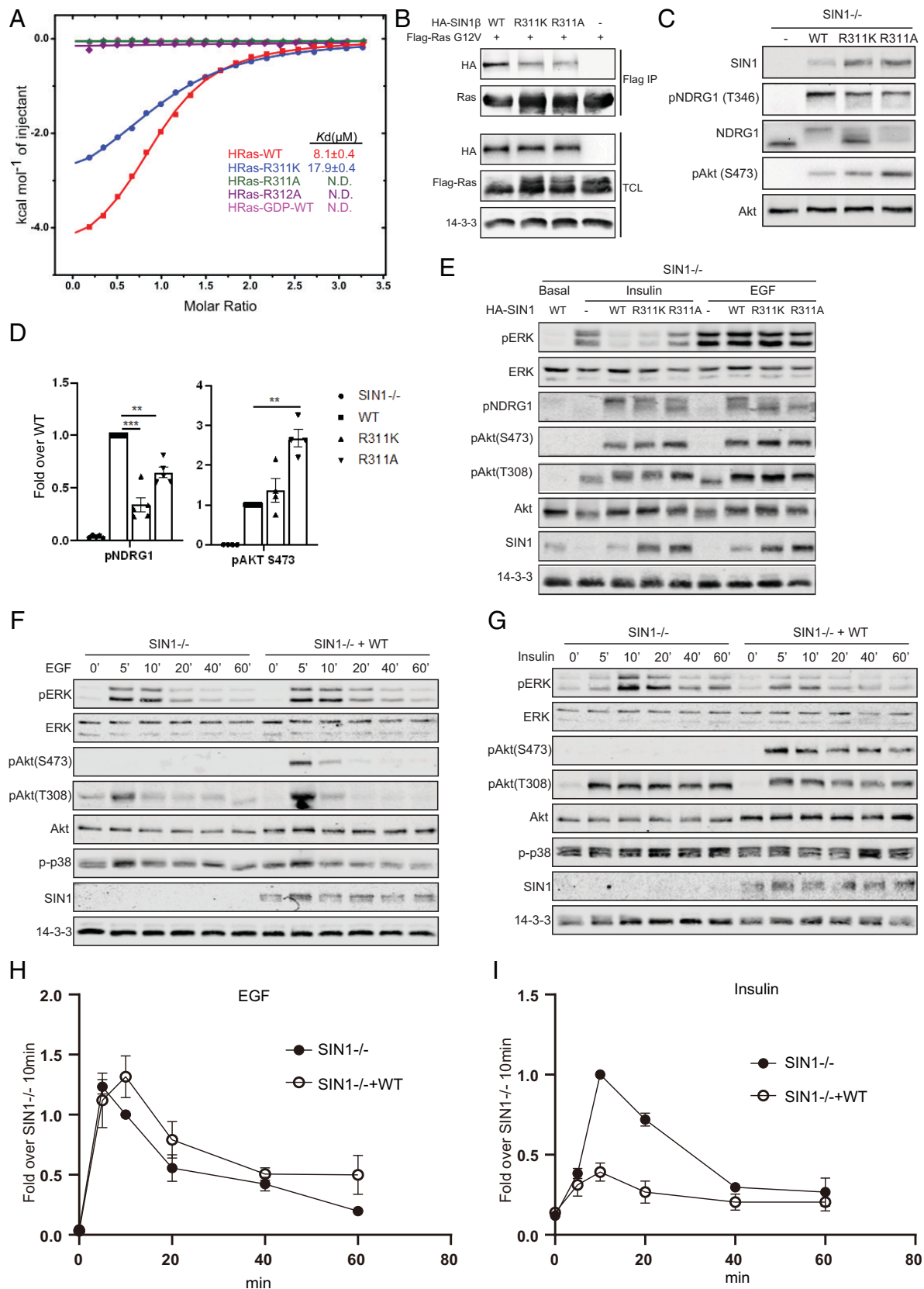


Fig. 2. Ras-SIN1 RBD interaction inhibits insulin-induced Ras signaling. (A) ITC titration results of WT or mutant SIN1 RBD with HRas-GMPNP. (B) Coimmunoprecipitation of HRas G12V with WT or mutant full-length SIN1 in MEF cells. (C) Immunoblot analysis of MEFs for mTORC2 downstream targets. (D) Graph shows means \pm SEM of densitometry analyses of the immunoblots in C normalized to total protein from three independent experiments, respectively. $***P < 0.01$, $****P < 0.001$; two-tailed Student's *t* test. (E) Expression of SIN1 suppresses insulin-induced but not EGF-induced ERK phosphorylation. (F and G) Immunoblot analysis of MEFs following different EGF (F) or insulin (G)-stimulated time points for proteins known to belong to the Ras pathway. (H and I) Graph shows means \pm SEM of densitometry analyses of the immunoblots in F and G normalized to total protein from three independent experiments, respectively.

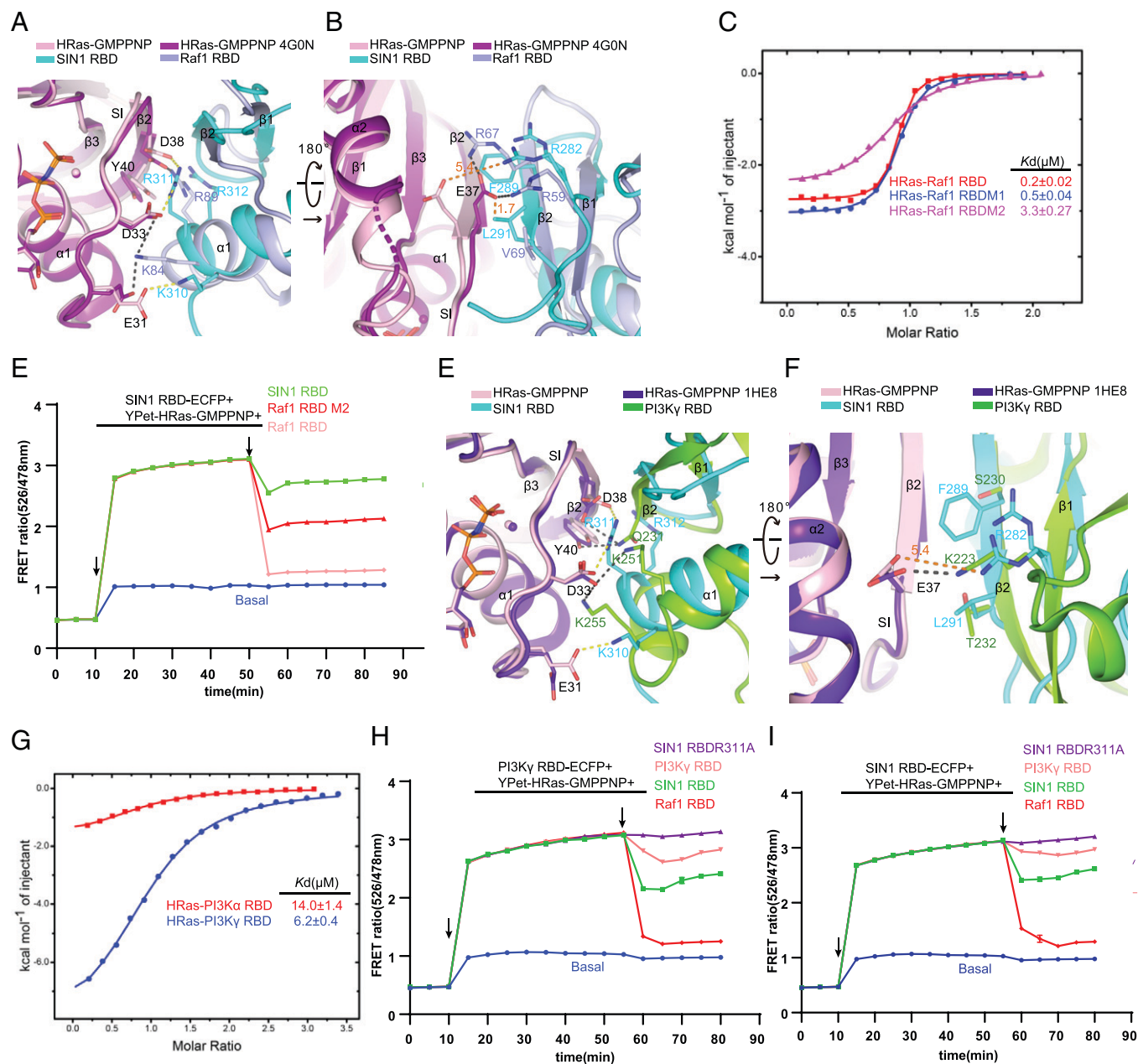


Fig. 3. Comparison of HRas-Raf1 RBD, HRas-PI3K γ RBD, and HRas-SIN1 RBD interactions. (A and B) Superposition of HRas-GMPPNP-Raf1 RBD structure (Protein data bank (PDB): 4G0N) with HRas-GMPPNP-SIN1 RBD structure. The rmsd between the two structures is 1.56 Å over 219 aligned C α atoms. Black dashed lines indicate salt bridges formed between HRas and Raf1 RBD, yellow dashed lines indicate salt bridges formed between HRas and SIN1 RBD, and orange dashed lines represent the distance (Å) between atoms. (C) ITC titration of Raf1 RBD with HRas GMPPNP. WT Raf1 RBD binds HRas with high affinity; R67F mutation (M1) slightly reduced the binding affinity; while R67F, V69L double mutation (M2) mimicking SIN1 RBD greatly weakened the interaction. (D) FRET competition assays with SIN1 RBD-ECFP and YPet-HRas-GMPPNP. Addition of equal molar amounts of nonfluorescent proteins (SIN1 RBD, Raf1 RBD, or Raf1 RBD M2) reduced the FRET between SIN1 RBD-ECFP and YPet-HRas-GMPPNP to different degrees. The blue line is the basal FRET between ECFP and YPet-HRas-GMPPNP. (E and F) Superposition of HRas-GMPPNP-PI3K γ structure (PDB: 1HE8) with HRas-GMPPNP-SIN1 RBD structure. The rmsd between the two structures is 1.35 Å over 205 aligned C α atoms. Black dashed lines indicate salt bridges or hydrogen bonds formed between HRas and PI3K γ RBD, yellow dashed lines indicate salt bridges formed between HRas and SIN1 RBD, and orange dashed lines represent the distance (Å) between atoms. (G) ITC titration of PI3K γ RBD (216 to 312) or PI3K α RBD (152 to 300) with HRas-GMPPNP. (H) FRET competition assays with PI3K γ RBD-ECFP and YPet-HRas-GMPPNP. Addition of equal molar amounts of nonfluorescent proteins (SIN1 RBD, SIN1 RBD R311A, PI3K γ RBD, Raf1 RBD) reduced the FRET between PI3K γ RBD-ECFP and YPet-HRas-GMPPNP to different degrees. (I) FRET competition assays with SIN1 RBD-ECFP and YPet-HRas-GMPPNP. Addition of equal molar amounts of nonfluorescent proteins as in H reduced the FRET between SIN1 RBD-ECFP and YPet-HRas-GMPPNP to different degrees.

and LY294002, but EGF-induced ERK1/2 phosphorylation was resistant to these inhibitors (29). Indeed, treatment with PI3K inhibitor, wortmannin, inhibited insulin-induced ERK phosphorylation and blunted the inhibitory effect of SIN1 (SI Appendix, Fig. S7 D and E). In contrast, Akt inhibition by MK2206 enhanced insulin-mediated ERK phosphorylation because Akt is

known to negatively regulate the Ras-ERK pathway (30–32). Thus, it is possible that SIN1-Ras interaction perturbed PI3K-related activities but not directly through Raf1.

It has been reported that SIN1 has multiple isoforms, one of which (SIN1- α) lacks amino acids 321 to 355, causing an incomplete RBD (33) (SI Appendix, Fig. S2). However, according to

our structural analysis, the key residues that play important roles in the Ras-SIN1 RBD interaction, such as R311 and R312, still exist in SIN1- α , indicating this isoform might still be able to interact with Ras. Indeed, SIN1- α was coimmunoprecipitated with HRas as much as full-length SIN1 (SIN1- β) (Fig. 4A). Surprisingly, compared to the two longer forms of SIN1, much more SIN1- γ , the shortest isoform with PH deletion, is precipitated together with Ras, either WT or G12V mutant (Fig. 4A). These data suggest the existence of autoinhibition on the Ras-SIN1 interaction by the SIN1 PH domain. To test this possibility, we generated a SIN1 fragment, RBD-PH containing both RBD and PH domains. As expected, this fragment binds to Ras with a much lower affinity ($K_d > 100 \mu\text{M}$) and GST-RBD-PH coprecipitates much less HRas than GST-RBD (Fig. 4B and C). It has been reported that the SIN1 PH domain suppresses

mTOR activity via interacting with the mTOR kinase domain (34). We hypothesized that the autoinhibition by PH is likely due to an intramolecular interaction with the RBD domain. Indeed, the results of the GST pulldown experiments showed that the PH, but not the CRIM domain can bind to the RBD in vitro (Fig. 4D). These data further validate the inhibitory effect of the SIN1 PH domain on Ras binding.

A large body of data have demonstrated that Ras proteins could form dimers or oligomers (nanoclusters) on the membrane and the oligomerization is critical for Ras function (35–39). Ras dimerization is mainly mediated by residues in $\alpha 4$ and $\alpha 5$ as shown by several groups and mutation in this region (e.g., D154Q) led to less ERK phosphorylation (35, 36, 40). In the crystals of HRas-SIN1 RBD, we found that HRas makes specific contacts with a symmetry-related HRas molecule

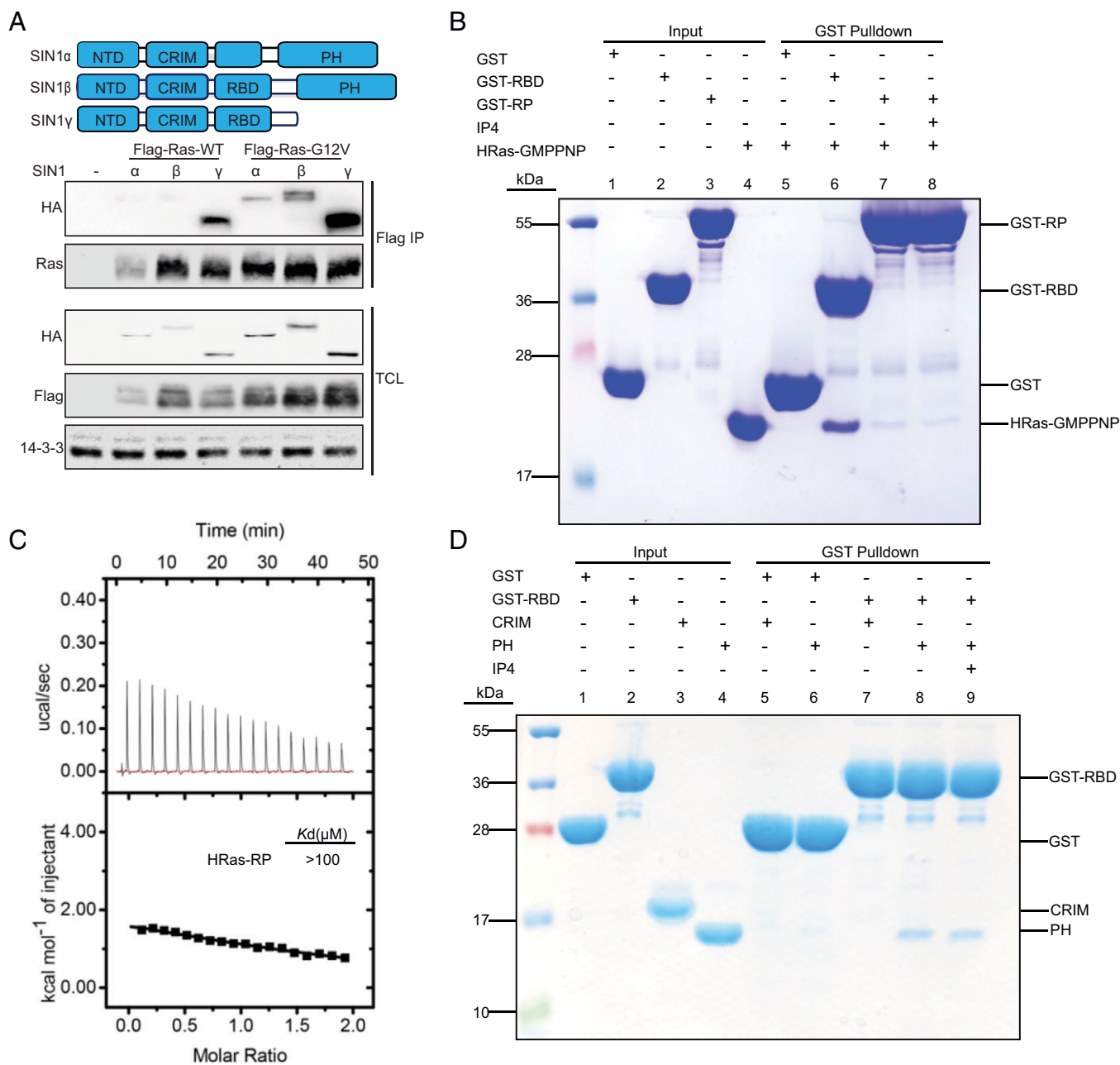


Fig. 4. SIN1 PH inhibits Ras-SIN1 RBD interaction. (A) Coimmunoprecipitation of SIN1 isoforms with WT or G12V HRas in MEF cells. (B) GST pull-down analysis of SIN1 RBD or RBD-PH (RP) with HRas-GMPPNP. RBD-PH binds HRas much weaker than RBD alone. Addition of $60 \mu\text{M}$ IP4 (the head group of PIP3) to the mixture had little effect on HRas RBD-PH interaction. (C) ITC titration of SIN1 RBD-PH (RP) with HRas-GMPPNP yielded a K_d greater than $100 \mu\text{M}$, indicating the affinity between the two is quite low. (D) GST pull-down assay showed that SIN1 RBD could associate with the PH domain but not CRIM.

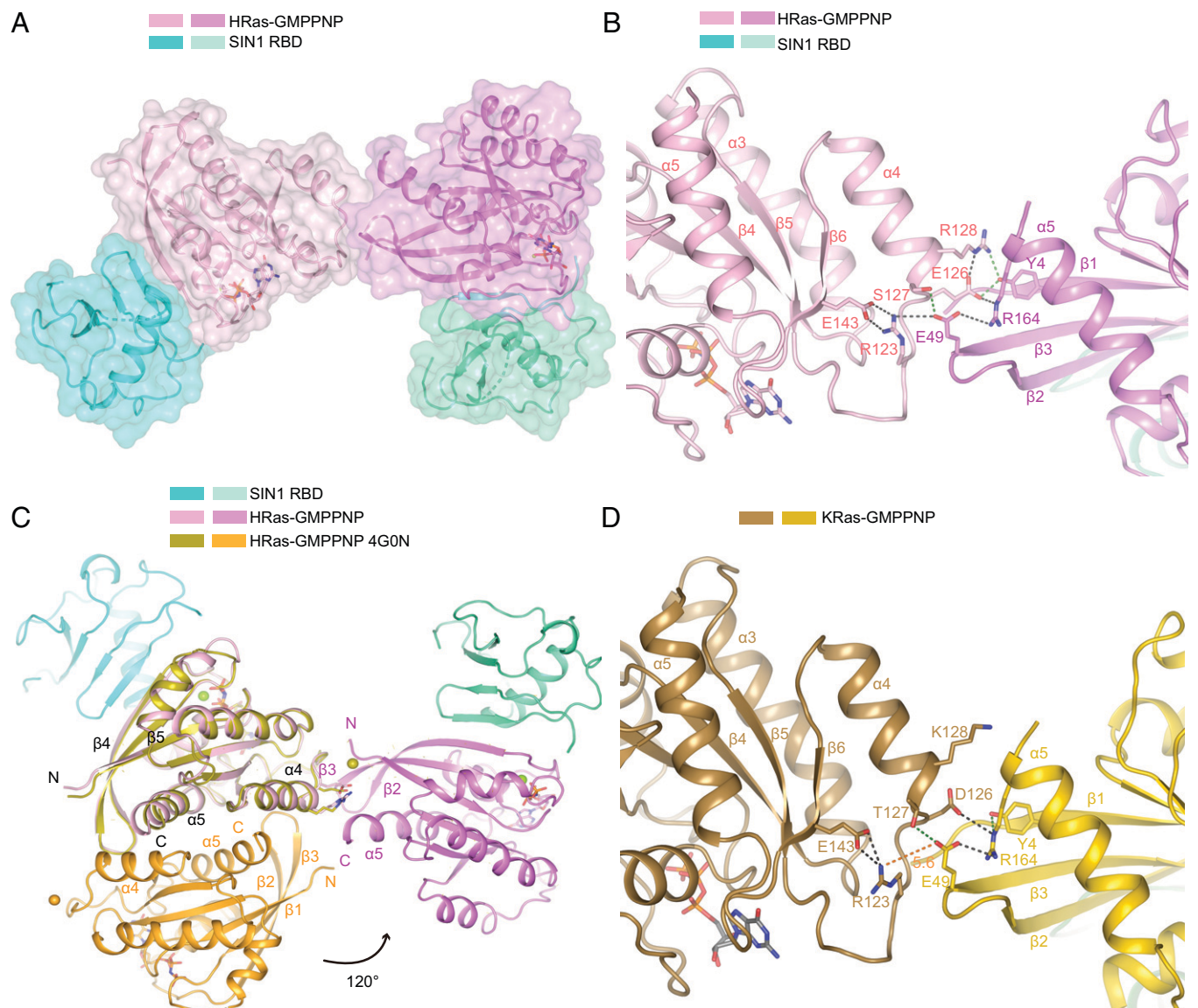


Fig. 5. Ras dimerization interface observed in crystal packing. (A) Surface diagram showing the observed HRas dimerization interface from HRas-SIN1 RBD crystal packing. Two Ras molecules are colored pink and magenta, respectively. (B) Close-up view of the Ras dimerization interface residues. Green dashed lines indicate hydrogen bonds, and black dashed lines denote salt bridges. (C) Comparison of the canonical HRas dimer (colored in gold and orange) from PDB: 4G0N with HRas dimer (colored in pink and magenta) in A. The canonical HRas dimer is folded inward through the $\alpha 4$ and $\alpha 5$ interface. In our structure the HRas molecule colored in magenta is rotated around 120° relative to the orange-colored HRas molecule in 4G0N, producing a side-by-side, open arrangement. E126 and R128 are shown as sticks, gold and orange spheres denote Ca^{2+} ions in 4G0N, and green spheres are Mg^{2+} ions. (D) Ribbon representation of KRas-KRas contacts. Green dashed lines indicate hydrogen bonds, black dashed lines denote salt bridges, and orange dashed lines represent the distance (\AA) between atoms.

employing a different interface (Fig. 5 A and B). E143-R123-E49-R164-E126-R128 formed a continuous electrostatic chain between two adjacent HRas molecules, while S127 and Y4 also contributed to the interaction through hydrogen bonds (Fig. 5 B). Previous studies showed that residues around $\alpha 4$ (R128) might be involved in membrane lipid binding or protein-protein interaction while the loop between $\beta 2$ and $\beta 3$ where E49 was located is involved in Ras dimerization (35, 36). Compared to the canonical HRas dimer (with $\alpha 4$ and $\alpha 5$ buried in the interface) observed in the HRas-Raf1 RBD (4G0N) crystal packing, the loop between $\beta 2$ and $\beta 3$ is rotated 120° to interact with $\alpha 4$ and the loop region before $\alpha 4$, overlapping with the calcium ion coordinated by E126 in 4G0N (Fig. 5 C), and the resulting side-by-side dimer is much more open compared to the previously described dimer (Fig. 5 C). The same Ras-Ras interface is also observed in KRas-SIN1 crystals; however, several residues here are different between KRas

and HRas. E49 in KRas is farther away from R123 and K128 is exposed to solvent (Fig. 5 D). Similar to the findings of several other groups (35, 37), we did not detect HRas G-domain dimers in solution due to the weak Ras-Ras affinity (*SI Appendix, Fig. S8*). Nevertheless, in 293T cells, overexpression of HRasG12V or KRasG12V with additional mutations in the dimer interface we observed (E49A, E126A in HRas; E49A, D126A in KRas4A) resulted in more ERK phosphorylation (*SI Appendix, Fig. S9 A and B*). It appears Ras dimerization through this interface plays a negative role for EGF-induced ERK activation.

Discussion

Ras proteins are key regulators of both the Ras/Raf/MEK/ERK and the PI3K/Akt/mTOR pathways and play a critical role in controlling cell growth. Oncogenic Ras proteins are found to

be in more than 25% of all cancer types (41). Under growth factor stimulation, Ras is able to directly bind to its effectors like Raf kinases or PI3Ks and activate their kinase activity. Although several studies confirmed the binding of SIN1 and Ras (11–13, 32), the function of this interaction remains controversial. Schroder et al. (13) reported that SIN1 suppressed Ras signaling, whereas a recent study showed the SIN1 mutant's inability to bind Ras does not affect MAPK signaling upon EGF stimulation (22). Here we found that SIN1 binding to Ras inhibits insulin-stimulated ERK activation but not EGF-stimulated ERK activation, which gives an explanation for previous controversial observations.

The different effect observed for insulin and EGF is surprising as both insulin and EGF could lead to the activation of the Ras/Raf/MEK/ERK pathway by recruitment of Grb2-SOS (guanine-nucleotide-exchange factor for Ras) through receptor kinase or adapter protein phosphorylation (30, 31, 42). The other common pathway activated by insulin/EGF is PI3K/AKT (30, 31, 43). The two dynamic signaling pathways are regulated by many context-dependent crosstalk and feedback loops (30, 31, 44). One critical crosstalk route is through phosphatidylinositol (3,4,5)-trisphosphate (PIP3) produced by activated PI3K. PIP3 recruits PH-domain-containing proteins like GAB (Grb2-associated binding partner) and IRS to the membrane, which recruits more Grb2-SOS to produce GTP-bound Ras (30, 31). Activated Ras could bind to PI3K and help stabilize PI3K at the membrane, resulting in more PI3K activation (44). A previous study with PI3K inhibitors in cancer cell lines showed that PI3K is required for insulin-stimulated but not EGF-stimulated ERK1/2 activation (29). It was also reported that in 293 cells EGF acts as a potent activator of the Ras/ERK pathway while the Ras/ERK pathway is poorly activated by insulin (45). It is plausible that insulin-mediated ERK activation relies more on a PI3K-dependent positive feedback loop (*SI Appendix, Fig. S10*). Our results in Fig. 3 show that SIN1 RBD could compete with PI3K RBDs for Ras binding in solution, and it is possible that SIN1 reduces PI3K activation by competitively binding to Ras and subsequently impairing the effect of the positive feedback loop of PI3K on Ras/Raf/ERK activation (*SI Appendix, Fig. S10*). Further studies will be required to pinpoint the exact extent of SIN1 on PI3K activities in cells. There are also possibilities that an insulin-specific outcome could be mediated by IRS1 phosphorylation level and its association with the Grb2-SOS or PI3K p85 subunit (30, 31, 45). The insulin receptor requires IRS proteins to interact with PI3K while some EGFR members like ERBB3 and ERBB4 directly bind and activate PI3K (43, 46). How IRS proteins are changed when SIN1/mTORC2 binds to Ras is also worth looking into in future studies.

SGK1 protein lacks the PH domain and is reported to localize to many cellular compartments including the plasma membrane, the nucleus, the endoplasmic reticulum, mitochondria, and cytoplasm (47, 48). Through analysis of NDRG1 phosphorylation, we found that SIN1 RBD mutations reduced SGK1 activity. This could be due to the combined but independent action of CRIM and RBD domains of SIN1. CRIM recruits SGK1 while RBD binds to Ras, and Ras in turn could stabilize SIN1/mTORC2-SGK1 at the plasma membrane. This is in agreement with previous studies showing SIN1/mTORC2 colocalized with activated HRas/KRas (13) and deletion of the C terminus of SIN1 (193–522) greatly reduced NDRG1 phosphorylation (14).

SIN1 PH domain is proposed to bind PIP3 and mediate mTORC2 membrane association and activation (34).

However, its exact role in regulating mTORC2 function is still debatable as it was reported that SIN1 PH domain could bind several kinds of phosphatidylinositol (13) and target mTORC2 to the membrane in a PIP3-independent manner (49). We showed that the PH domain has an inhibitory effect on SIN1-Ras binding. Castel et al. (22) reported the same conclusion. Further studies would be required to reveal what triggers the PH domain to release its inhibitory effect on Ras-SIN1 interaction.

Recently Senoo et al. (50) found that in response to insulin, phosphorylated GTP-KRas4B and GDP-RhoA form a super-complex (KARATE) with mTORC2, and the association with mTORC2/SIN1 is proposed to be through GDP-RhoA while GTP-KRas4B binds to GDP-RhoA. However, it is not clear whether GTP-KRas4B directly associates with mTORC2 in their results. In our in vitro experiments we failed to detect binding between SIN1 RBD and the G domain of RhoA-GMPPNP or RhoA-GDP (Fig. 1B). It is possible that the intact mTORC2 is required for binding RhoA and the detailed interaction mechanism would require further investigation.

During preparation of this paper, Castel et al. (22) reported the structures of KRas4B(Q61R) mutant in complex with SIN1 RBD (PDB: 7LC2) and KRas4B(Q25A) mutant in complex with the SIN1 RBD-PH (PDB: 7LC1). Superposition of WT KRas4A-SIN1 RBD structure (this study) with KRas4B(Q61R)-SIN1 RBD structure (PDB: 7LC2) produced an rmsd of 0.81 Å over 240 aligned C α atoms (*SI Appendix, Fig. S11A*). The positions of residues involved in intermolecular interaction are almost identical. Superposition of WT KRas4A-SIN1 RBD structure (this study) with KRas4B(Q25A)-SIN1 RBD-PH structure (PDB: 7LC1) produced an rmsd of 0.88 Å over 241 aligned C α atoms (*SI Appendix, Fig. S11B*). In 7LC1 structure, the α 2 helix of KRas is in contact with the linker helix between the RBD and PH domains in SIN1 (the linker helix is where KRas interacts with SIN1 besides the RBD domain). In our WT KRas4A structure, the α 2 helix of KRas has the same sequence as KRas4B in 7LC1 and adopts nearly identical conformation (*SI Appendix, Figs. S1 and S11B*). The α 2 helix in HRas also has the same sequence as KRas and adopts a similar conformation (*SI Appendix, Figs. S1 and S11C*), so it is very likely that HRas interacts with the linker helix the same way as KRas. As mentioned earlier, the effector lobe for HRas or KRas to interact with SIN1 RBD has the same sequence, and it makes sense that HRas and KRas G domains both interact with SIN1 in vitro.

While the recent study found only KRas G12V interacts with SIN1 RBD in cells (22), we demonstrated that in cells HRas also interacts with the SIN1, in agreement with the results from previous studies (13, 14). It is notable that in cells HRas interacts weakly with full-length SIN1 as shown by the Co-IP results, and in vitro HRas has a weak affinity for RBD-PH. However, it is evident that the SIN1- γ isoform associates strongly with HRas (Fig. 4A), indicating the PH domain might serve a critical regulation role for Ras association with SIN1. It is also worth mentioning that the allosteric lobe and especially the HVR region are quite divergent among different Ras isoforms, which might contribute to isoform-specific functions.

A plethora of biochemical, structural, single-molecule, and molecular dynamic simulation studies of the Ras-Raf signaling complex revealed that Raf kinase complex binding to Ras promotes Ras dimerization and subsequent binding of Galectin dimers to form an intricate signalosome to activate a downstream kinase cascade (35–40, 51–54). Strong evidence supports the notion that both HRas and KRas could dimerize

through the $\alpha 4$ and $\alpha 5$ interface and disruption of the interface residues leads to reduced Raf activity (35–37, 40). However, the high-order Ras assembly on membrane remains vague because of the dynamic nature of the signaling events. As often seen in studies of membrane-bound proteins, even very weak interactions in solution could have a huge impact on protein activity on the two-dimensional (2D) membrane. A recent structural and molecular dynamics simulation study of KRas4B-Raf1 RBDCRD (CRD, cysteine-rich domain) showed that monomeric KRas-Raf1 RBDCRD complex could use $\alpha 4$ and $\alpha 5$ to interact with membrane (55–57). This is different from previously proposed modes of KRas dimerization involving $\alpha 4$ and $\alpha 5$ and might reflect membrane-induced Ras reorganization. Interestingly, the dimerization interface we observed in this study is actually compatible with $\alpha 4$ and $\alpha 5$ interacting with membrane while maintaining dimer conformation (Fig. 5 A and C). The $\alpha 4$ and $\alpha 5$ helices in both Ras molecules are now exposed.

The results of the mutational study we carried out in *SI Appendix, Fig. S9* are in line with previous studies demonstrating that HRas E49, together with D47, could affect Ras membrane orientation and E49A D47A double mutation enhanced ERK phosphorylation while D47A alone led only to minor changes in ERK phosphorylation (58–60). Investigation of KRas4B interaction with phosphatidylinositol (4, 5)-phosphate (PIP2) containing lipid found that KRas E49K showed reduced lipid association and increased transforming activity (61). So it is likely the dimerization interface we observed might be linked to Ras membrane association.

Intriguingly, the dimer we observed is in a head-to-tail fashion and if the oligomerization is extended further, we get a right-handed helical assembly, with six Ras molecules per turn and a helical pitch around 124 Å (*SI Appendix, Fig. S12 A–C*). The inside diameter is around 50 Å and lined with $\alpha 4$, $\alpha 5$, and $\beta 6$ residues (*SI Appendix, Fig. S12 A–C*). SIN1 RBD or SIN1 RBD-PH can be fitted to this assembly with no steric clashes (*SI Appendix, Fig. S12 A–D*). Similarly, we superposed the KRas-Raf1 RBDCRD structure (PDB: 6XI7) to the KRas dimer we observed in Fig. 5D and found there is no obvious clash in the helical assembly either (*SI Appendix, Fig. S13 A–C*). Mysore et al. (38) recently proposed a helical assembly model for KRas, in which the GMA (GTP-mediated asymmetric) KRas dimer they used as a starting model for simulation led to a left-handed helix. The GMA dimer itself is rare and formed in only 5% of simulations (38). The negative stain electron microscopy results from Mysore et al. (38) with full-length KRas on lipid monolayer indeed displayed ring-shaped 2D classes, compatible with a helical arrangement. However, it is not possible to distinguish the handedness from top view 2D projections. These discrepancies and the importance of Ras high-order organization definitely warrant further investigation of full-length proteins on membranes or lipid bilayers.

In summary, in this study we solved the high-resolution structures of H/KRas-SIN1 RBD complexes, revealing the binding mode of these two important effectors from MAPK and mTORC2 signaling pathways. We found that SIN1 association with Ras induces more SGK1 activation. In addition, SIN1 interacts with Ras to suppress ERK signaling in response to specific growth factors like insulin and this interaction can be inhibited by the SIN1 PH domain. The different response to insulin or EGF might be attributed to SIN1 competing with PI3K for Ras binding and the intrinsic signaling difference between insulin and EGF. Furthermore, a potential Ras dimerization interface was uncovered through crystal packing analysis. Together, these results provide a snapshot of crosstalk between the mTORC2 pathway and the Ras/ERK pathway and lay the foundation for future research.

Materials and Methods

To overcome the weak affinity between SIN1 RBD and Ras and facilitate crystallization, a short flexible linker (TGSMG) was introduced between SIN1 RBD (272 to 360) and HRas or KRas G domain (1 to 166). Crystals of GMPPNP-bound HRas-SIN1 RBD, HRasG12V-SIN1 RBD, HRasQ61L-SIN1 RBD, and KRas-SIN1 RBD diffracted to ~1.6 to 1.7 Å. Data were indexed, integrated, and scaled using the XDS, CCP4 program Pointless and Aimless (62–64). The structures of HRas-SIN1 RBD, HRasG12V-SIN1 RBD, HRasQ61L-SIN1 RBD, and KRas-SIN1 RBD were determined by molecular replacement using the HRas structure from PDB 4GON (25) as an initial searching model with Phaser (65). The structural models were built using Coot (66) and refined using PHENIX (67). The linker residues for protein fusion were not observed in the electron density map, indicating they are flexible and not affecting protein interaction. The statistics of the data collection and refinement are shown in *SI Appendix, Table S1*. A detailed description of materials and methods can be found in *SI Appendix*.

Data Availability. The atomic coordinates and structure factors have been deposited in the Research Collaboratory for Structural Bioinformatics Protein Data Bank (RCSB PDB, <https://www.rcsb.org/>) with the following accession codes: 7VVB (SIN1 RBD-KRas4A), 7VVG (SIN1 RBD-HRasG12V), 7VW8 (SIN1 RBD-HRasQ61L), and 7WV9 (SIN1 RBD-HRas).

ACKNOWLEDGMENTS. We thank the beamline staff of BL17U1 and BL19U1at Shanghai Synchrotron Radiation Facility for help with data collection and Prof. Jiamu Du and Dr. Jianlong Yuan for help with ITC experiments. We thank Prof. Bing Su and Prof. Estela Jacinto for sharing SIN1 KO MEFs and Dr. Wayne Schroder and Prof. Gillian Bushell for sharing SIN1 constructs. This work was supported by Australia National Health and Medical Research Council (NHMRC) project Grant GNT1120201 (to D.E.J.) and National Science Foundation of China Grant 31971125 (to C.Z.). D.E.J. is an NHMRC Senior Principal Research Fellow. G.Y. was supported by an NHMRC early-career fellowship.

Author affiliations: ^aSchool of Public Health, Zhejiang University School of Medicine, Hangzhou, 310058, China; ^bSir Run Run Shaw Hospital, Zhejiang University School of Medicine, Hangzhou, 310016, China; ^cDepartment of Cell Biology, Zhejiang University School of Medicine, Hangzhou, 310058, China; ^dSchool of Life and Environmental Sciences, The Charles Perkins Centre, The University of Sydney, Sydney, NSW 2006, Australia; and ^eSydney Medical School, The University of Sydney, Sydney, NSW 2006, Australia

1. C. Betz, M. N. Hall, Where is mTOR and what is it doing there? *J. Cell Biol.* **203**, 563–574 (2013).
2. I. Ben-Sahra, B. D. Manning, mTORC1 signaling and the metabolic control of cell growth. *Curr. Opin. Cell Biol.* **45**, 72–82 (2017).
3. R. A. Saxton, D. M. Sabatini, mTOR signaling in growth, metabolism, and disease. *Cell* **168**, 960–976 (2017).
4. S. G. Kim, G. R. Buel, J. Blenis, Nutrient regulation of the mTOR complex 1 signaling pathway. *Mol. Cells* **35**, 463–473 (2013).
5. W. Fu, M. N. Hall, Regulation of mTORC2 signaling. *Genes (Basel)* **11**, 1045 (2020).
6. L. J. Saucedo et al., Rheb promotes cell growth as a component of the insulin/TOR signalling network. *Nat. Cell Biol.* **5**, 566–571 (2003).
7. H. Stocker et al., Rheb is an essential regulator of S6K in controlling cell growth in Drosophila. *Nat. Cell Biol.* **5**, 559–565 (2003).
8. E. Kim, P. Goraksha-Hicks, L. Li, T. P. Neufeld, K. L. Guan, Regulation of TORC1 by Rag GTPases in nutrient response. *Nat. Cell Biol.* **10**, 935–945 (2008).
9. Y. Sancak et al., The Rag GTPases bind raptor and mediate amino acid signaling to mTORC1. *Science* **320**, 1496–1501 (2008).
10. G. Yang et al., RagC phosphorylation autoregulates mTOR complex 1. *EMBO J.* **38**, e99548 (2019).
11. J. Colicelli et al., Expression of three mammalian cDNAs that interfere with RAS function in *Saccharomyces cerevisiae*. *Proc. Natl. Acad. Sci. U.S.A.* **88**, 2913–2917 (1991).
12. S. Lee, C. A. Parent, R. Insall, R. A. Firtel, A novel Ras-interacting protein required for chemotaxis and cyclic adenosine monophosphate signal relay in Dictyostelium. *Mol. Biol. Cell* **10**, 2829–2845 (1999).
13. W. A. Schroder et al., Human Sin1 contains Ras-binding and pleckstrin homology domains and suppresses Ras signalling. *Cell. Signal.* **19**, 1279–1289 (2007).
14. J. R. Kovalski et al., The functional proximal proteome of oncogenic Ras includes mTORC2. *Mol. Cell* **73**, 830–844.e12 (2019).
15. E. Jacinto et al., SIN1/MIP1 maintains rictor-mTOR complex integrity and regulates Akt phosphorylation and substrate specificity. *Cell* **127**, 125–137 (2006).

16. Q. Yang, K. Inoki, T. Ikenoue, K. L. Guan, Identification of Sin1 as an essential TORC2 component required for complex formation and kinase activity. *Genes Dev.* **20**, 2820–2832 (2006).
17. S. J. Humphrey *et al.*, Dynamic adipocyte phosphoproteome reveals that Akt directly regulates mTORC2. *Cell Metab.* **17**, 1009–1020 (2013).
18. G. Yang, D. S. Murashige, S. J. Humphrey, D. E. James, A positive feedback loop between Akt and mTORC2 via SIN1 phosphorylation. *Cell Rep.* **12**, 937–943 (2015).
19. M. A. Frias *et al.*, mSin1 is necessary for Akt/PKB phosphorylation, and its isoforms define three distinct mTORC2s. *Curr. Biol.* **16**, 1865–1870 (2006).
20. A. Scaiola *et al.*, The 3.2-Å resolution structure of human mTORC2. *Sci. Adv.* **6**, eabc1251 (2020).
21. G. Buhman, G. Holzapfel, S. Fetics, C. Mattos, Allosteric modulation of Ras positions Q61 for a direct role in catalysis. *Proc. Natl. Acad. Sci. U.S.A.* **107**, 4931–4936 (2010).
22. P. Castel *et al.*, RAS interaction with Sin1 is dispensable for mTORC2 assembly and activity. *Proc. Natl. Acad. Sci. U.S.A.* **118**, e2103261118 (2021).
23. H. Tatebe *et al.*, Substrate specificity of TOR complex 2 is determined by a ubiquitin-fold domain of the Sin1 subunit. *eLife* **6**, e19594 (2017).
24. C. Wellbrock, M. Karasarides, R. Marais, The RAF proteins take centre stage. *Nat. Rev. Mol. Cell Biol.* **5**, 875–885 (2004).
25. S. K. Fetics *et al.*, Allosteric effects of the oncogenic RasQ61L mutant on Raf-RBD. *Structure* **23**, 505–516 (2015).
26. A. Sjölander, K. Yamamoto, B. E. Huber, E. G. Lapetina, Association of p21ras with phosphatidylinositol 3-kinase. *Proc. Natl. Acad. Sci. U.S.A.* **88**, 7908–7912 (1991).
27. A. A. Krygowska, E. Castellano, PI3K: A crucial piece in the RAS signaling puzzle. *Cold Spring Harb. Perspect. Med.* **8**, a031450 (2018).
28. M. E. Pacold *et al.*, Crystal structure and functional analysis of Ras binding to its effector phosphoinositide 3-kinase gamma. *Cell* **103**, 931–943 (2000).
29. L. Liu, Y. Xie, L. Lou, PI3K is required for insulin-stimulated but not EGF-stimulated ERK1/2 activation. *Eur. J. Cell Biol.* **85**, 367–374 (2006).
30. M. C. Mendoza, E. E. Er, J. Blenis, The Ras-ERK and PI3K-mTOR pathways: Cross-talk and compensation. *Trends Biochem. Sci.* **36**, 320–328 (2011).
31. E. Aksamitiene, A. Kiyatkin, B. N. Kholodenko, Cross-talk between mitogenic Ras/MAPK and survival PI3K/Akt pathways: A fine balance. *Biochem. Soc. Trans.* **40**, 139–146 (2012).
32. B. D. Manning, A. Toker, AKT/PKB signaling: Navigating the network. *Cell* **169**, 381–405 (2017).
33. Y. Yuan *et al.*, Characterization of Sin1 isoforms reveals an mTOR-dependent and independent function of Sin1γ. *PLoS One* **10**, e0135017 (2015).
34. P. Liu *et al.*, PtdIns(3,4,5)P3-dependent activation of the mTORC2 kinase complex. *Cancer Discov.* **5**, 1194–1209 (2015).
35. J. Guldnhaupt *et al.*, N-Ras forms dimers at POPC membranes. *Biophys. J.* **103**, 1585–1593 (2012).
36. X. Nan *et al.*, Ras-GTP dimers activate the mitogen-activated protein kinase (MAPK) pathway. *Proc. Natl. Acad. Sci. U.S.A.* **112**, 7996–8001 (2015).
37. M. R. Packer *et al.*, Raf promotes dimerization of the Ras G-domain with increased allosteric connections. *Proc. Natl. Acad. Sci. U.S.A.* **118**, e2015648118 (2021).
38. V. P. Mysore *et al.*, A structural model of a Ras-Raf signalosome. *Nat. Struct. Mol. Biol.* **28**, 847–857 (2021).
39. W. C. Lin *et al.*, H-Ras forms dimers on membrane surfaces via a protein-protein interface. *Proc. Natl. Acad. Sci. U.S.A.* **111**, 2996–3001 (2014).
40. C. Ambrogio *et al.*, KRAS dimerization impacts MEK inhibitor sensitivity and oncogenic activity of mutant KRAS. *Cell* **172**, 857–868.e15 (2018).
41. G. A. Hobbs, C. J. Der, K. L. Rossman, RAS isoforms and mutations in cancer at a glance. *J. Cell Sci.* **129**, 1287–1292 (2016).
42. P. A. Boriack-Sjodin, S. M. Margarit, D. Bar-Sagi, J. Kuriyan, The structural basis of the activation of Ras by Sos. *Nature* **394**, 337–343 (1998).
43. B. D. Hopkins, M. D. Goncalves, L. C. Cantley, Insulin-PI3K signalling: An evolutionarily insulated metabolic driver of cancer. *Nat. Rev. Endocrinol.* **16**, 276–283 (2020).
44. S. F. Smith, S. E. Collins, P. G. Charest, Ras, PI3K and mTORC2 - Three's a crowd? *J. Cell Sci.* **133**, jcs234930 (2020).
45. N. Borisov *et al.*, Systems-level interactions between insulin-EGF networks amplify mitogenic signaling. *Mol. Syst. Biol.* **5**, 256 (2009).
46. P. Wee, Z. Wang, Epidermal growth factor receptor cell proliferation signaling pathways. *Cancers (Basel)* **9**, 52 (2017).
47. B. Zhao *et al.*, Crystal structure of the kinase domain of serum and glucocorticoid-regulated kinase 1 in complex with AMP PNP. *Protein Sci.* **16**, 2761–2769 (2007).
48. N. S. Raikwar, P. M. Snyder, C. P. Thomas, An evolutionarily conserved N-terminal Sgk1 variant with enhanced stability and improved function. *Am. J. Physiol. Renal Physiol.* **295**, F1440–F1448 (2008).
49. M. Ebner, B. Sinkovics, M. Szczygiel, D. W. Ribeiro, I. Yudushkin, Localization of mTORC2 activity inside cells. *J. Cell Biol.* **216**, 343–353 (2017).
50. H. Senoo *et al.*, KARATE: PKA-induced KRAS4B-RHOA-mTORC2 supercomplex phosphorylates AKT in insulin signaling and glucose homeostasis. *Mol. Cell* **81**, 4622–4634.e8 (2021).
51. S. Muratcioglu *et al.*, GTP-dependent K-Ras dimerization. *Structure* **23**, 1325–1335 (2015).
52. T. Cooks, C. Mattos, Crystal structure reveals the full Ras-Raf interface and advances mechanistic understanding of Raf activation. *Biomolecules* **11**, 996 (2021).
53. E. Park *et al.*, Architecture of autoinhibited and active BRAF-MEK1-14-3-3 complexes. *Nature* **575**, 545–550 (2019).
54. Y. Kondo *et al.*, Cryo-EM structure of a dimeric B-Raf:14-3-3 complex reveals asymmetry in the active sites of B-Raf kinases. *Science* **366**, 109–115 (2019).
55. Z. Fang *et al.*, Multivalent assembly of KRAS with the RAS-binding and cysteine-rich domains of CRAF on the membrane. *Proc. Natl. Acad. Sci. U.S.A.* **117**, 12101–12108 (2020).
56. C. Neale, A. E. García, The plasma membrane as a competitive inhibitor and positive allosteric modulator of KRAS4B signaling. *Biophys. J.* **118**, 1129–1141 (2020).
57. T. H. Tran *et al.*, KRAS interaction with RAF1 RAS-binding domain and cysteine-rich domain provides insights into RAS-mediated RAF activation. *Nat. Commun.* **12**, 1176 (2021).
58. D. Abankwa *et al.*, A novel switch region regulates H-Ras membrane orientation and signal output. *EMBO J.* **27**, 727–735 (2008).
59. A. A. Gorfe, B. J. Grant, J. A. McCammon, Mapping the nucleotide and isoform-dependent structural and dynamical features of Ras proteins. *Structure* **16**, 885–896 (2008).
60. M. Solman *et al.*, Specific cancer-associated mutations in the switch III region of Ras increase tumorigenicity by nanocluster augmentation. *eLife* **4**, e08905 (2015).
61. S. Cao *et al.*, K-Ras G-domain binding with signaling lipid phosphatidylinositol (4,5)-phosphate (PIP2): Membrane association, protein orientation, and function. *J. Biol. Chem.* **294**, 7068–7084 (2019).
62. P. R. Evans, G. N. Murshudov, How good are my data and what is the resolution? *Acta Crystallogr. D Biol. Crystallogr.* **69**, 1204–1214 (2013).
63. W. Kabsch, XDS. *Acta Crystallogr. D Biol. Crystallogr.* **66**, 125–132 (2010).
64. M. D. Winn *et al.*, Overview of the CCP4 suite and current developments. *Acta Crystallogr. D Biol. Crystallogr.* **67**, 235–242 (2011).
65. A. J. McCoy *et al.*, Phaser crystallographic software. *J. Appl. Cryst.* **40**, 658–674 (2007).
66. P. Emsley, K. Cowtan, Coot: Model-building tools for molecular graphics. *Acta Crystallogr. D Biol. Crystallogr.* **60**, 2126–2132 (2004).
67. D. Liebschner *et al.*, Macromolecular structure determination using X-rays, neutrons and electrons: Recent developments in Phenix. *Acta Crystallogr. D Struct. Biol.* **75**, 861–877 (2019).